Available online at www.sciencedirect.com

ScienceDirect

International Journal of Solids and Structures 44 (2007) 399–418

INTERNATIONAL JOURNAL OF SOLIDS and STRUCTURES

www.elsevier.com/locate/ijsolstr

Elastic–plastic analysis of offset indentations on unpressurised pipes

T.H. Hyde, R. Luo, A.A. Becker *

School of Mechanical, Materials and Manufacturing Engineering, University of Nottingham, University Park, Nottingham NG7 2RD, UK

Received 16 November 2005; received in revised form 21 April 2006
Available online 16 May 2006

Abstract

The results of investigations to determine the elastic–plastic behaviour of unpressurised pipes with long offset indentations and unsymmetric support conditions are presented in this paper. They include the results of experimental tests, FE analyses and analytical methods. Three different materials and five different geometries are used to investigate their effects on the behaviour. A comparison of the experimental results, FE and analytical solutions indicates that the general analytical formulation developed in this paper for predicting the peak indenter loads in offset indented pipes, is reasonably accurate. Also, the analyses presented in this paper indicate that using a representative nominal flow stress, which is the average of yield and ultimate tensile stresses, in the analytical method, is appropriate for predicting the peak indenter loads.

Keywords: Indentation; Plasticity; Limit load; Pressurised pipes; Finite element analysis

1. Introduction

Buried pipelines are widely used for transmitting gases and liquids from their production sites to houses and industrial organisations. The safety of gas pipelines is of considerable concern within the gas industry due to the dangers associated with potential leaks and rupture. Indentation damage caused by diggers and earth movement can have a serious effect on the structural integrity of a pipe and can result in leak or rupture. The indentation of pipelines has therefore been the subject of research for many years, e.g., Corder and Chatain (1995), Fowler et al. (1995), Park and Kyriakides (1996), Kiefner et al. (1996), Lancaster and Palmer (1996a,b), Clapham et al. (1998), Doglione and Firrao (1998), Leis et al. (1998) and Alexander (1999).

Most impact damage to pipelines is very localised. However, in some cases, the damage can extend over a significant length of the pipe, see, e.g., (Alexander, 1999; Hyde et al., 2005a,b), where the behaviour, except at ends of the damage zone, is essentially two dimensional and can be analysed as a two-dimensional plane strain ring.

* Corresponding author. Tel.: +44 115 951 3791; fax: +44 115 951 3800.
E-mail address: a.a.becker@nottingham.ac.uk (A.A. Becker).

0020-7683/$ - see front matter
doi:10.1016/j.ijsolstr.2006.04.040

Nomenclature

α	angular position
$\alpha_1, \alpha_2, \alpha_3, \alpha_4, \alpha_5$	angles of rotation of the plastic hinges
δ	deflection/dent depth at the top centre of pipe/ring
θ_1	indentation angular offset position
$\theta_2, \theta_5, \theta_3, \theta_4$	angular positions of the supports and hinges
$\sigma_y, \sigma_f, \sigma_{UTS}$	yield, flow and ultimate tensile stresses
D	outer diameter of the pipe/ring
F	indenter force
F_U	upper bound to limit load
L	axial length of a dented ring
$L_s(\theta_1, \theta_2, \theta_5)$	normalised function
M_0	limit moment, defined as $\sigma_y t^2/4$
R	mean radius of the pipe/ring
t	wall thickness
W_I	internal energy dissipated
W_E	work done by the force F

The authors of this paper have investigated the limit load and force–deflection predictions of dented rings, with symmetrical supports, subject to symmetrical radial indenter loading for unpressurised (Hyde et al., 2005a) and pressurised pipes (Hyde et al., 2005b) using experimental tests, analytical methods and FE analyses. Previous work for pipes with symmetric supports (Hyde et al., 2005a,b) has shown that internal pressure causes the pipe to become much stiffer than the unpressurised pipe, and the analytical solutions for pressurised pipes are generally more complicated. In this paper, only the effects of unsymmetric supports and loading conditions on the indenter limit load for unpressurised pipes are investigated using experimental tests, FE analyses and analytical methods. Pressurised pipes with offset indentation are covered in another publication (Hyde et al., 2006).

For underground pipelines, the surrounding soil produces support for the pipelines and produces reaction forces that resist the pipeline deformation or the movements caused by indentation loads. Exact simulation of the support conditions produced by the surrounding soil is difficult and would require many experimental tests and corresponding FE and/or analytical analyses to be performed. In this paper, a general analytical formulation, which covers the effects of the support and indentation positions on the limit loads of indented rings, is described.

The indentation type investigated in this paper is shown in Fig. 1. If the offset indentation angle, θ_1, is zero, the indentation is radial with unsymmetric support conditions. Symmetric indentation conditions, in which

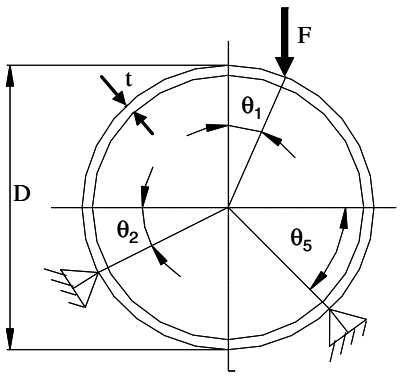

Fig. 1. Indentation loading and support conditions.

equal right and left support angles ($\theta_2 = \theta_5$) and zero offset indentation angle ($\theta_1 = 0°$) exist, have been covered in previous publications for unpressurised (Hyde et al., 2005a) and pressurised pipes (Hyde et al., 2005a). The objective of this work is to extend the previous work on FE and analytical solutions for a radial pipe indentation with symmetrical supports to cover more practical offset unsymmetrical indentations. The radial indentation may be considered as a special case of the offset indentation.

2. Experimental work and validation of the FE analyses

2.1. Material

The material chosen for the experimental investigation is 6082-T6 aluminium alloy. The tensile stress–strain curve for the material is shown in Fig. 2; Young's modulus, Poisson's ratio, yield stress and ultimate tensile stress are given in Table 1. Fig. 2 also shows the stress–strain curve for a practical gas pipeline material, namely X65 SAW. The material properties for 6082-T6 aluminium alloy, X65 SAW steel and an idealised elastic–plastic material (Ideal-A) are given in Table 1.

2.2. Geometry and loading

In order to perform the experimental tests for unsymmetric supports, 6082-T6 aluminium alloy rings were placed on a V-block, and plaster, which was cast into the gap between the rings and the V-block, was used to form an arc supporting bed, as shown in Fig. 3. The rings were also clamped to the V-block at position F. These support conditions provide an arc support. The support angles, θ_2 and θ_5 (55° and 35°, respectively) are shown in Fig. 3. Radial indentation, i.e., $\theta_1 = 0°$, was used. The rings were radially loaded at point A by a Bright Drawn Mild Steel indenter with an end radius of 2 mm and an axial length of 50 mm.

The tests were conducted on an Instron 1195 uniaxial test machine with 1 kN and 50 kN load cells. The load point displacement rate was set to 2 mm/min and the data (force and displacement) were recorded automatically. Tests were performed on four rings with the dimensions given in Table 2. Also given in Table 2 are the peak indenter loads obtained during the tests. The peak loads, or limit loads, were obtained from the maximum load point of the indenter force (per unit length of the pipe) versus dent depth curves, as shown in Fig. 4.

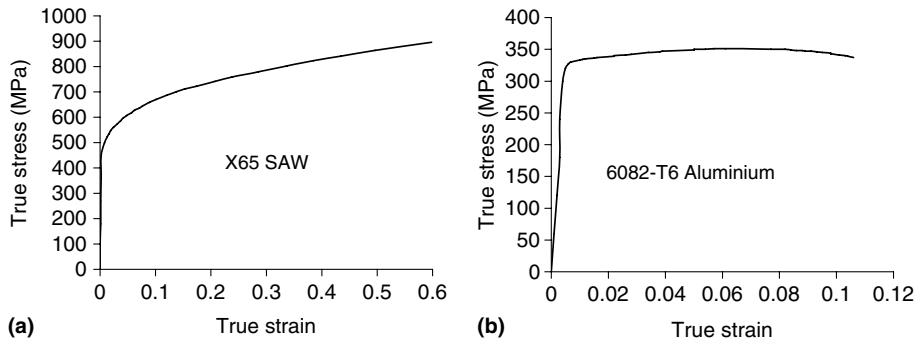

Fig. 2. True stress–strain curves of 6082-T6 aluminium alloy and X65 SAW pipe steel.

Table 1
Material parameters used in experiment tests

Material	E (GPa)	σ_y (MPa)	σ_{UTS} (MPa)	Poisson's ratio
6082-T6 alloy	70	300	351	0.3
X65 SAW	223	448	675	0.3
Ideal-A	70	300	×	0.3

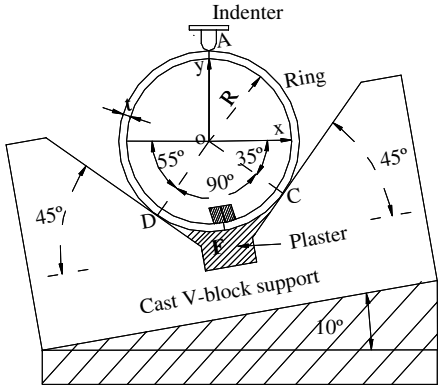

Fig. 3. Dented ring test conditions.

Table 2
Geometries and experimental peak load results for 6082-T6 aluminium alloy dented ring tests

Test no.	D (mm)	t (mm)	D/t	L (mm)	Peak load/unit length (N/mm)
TE1	120	1.5	80.0	50	14.9
TE2	125	3	41.6	50	64.0
TE3	120	5	24	50	203
TE4	120	5	24	50	200.3

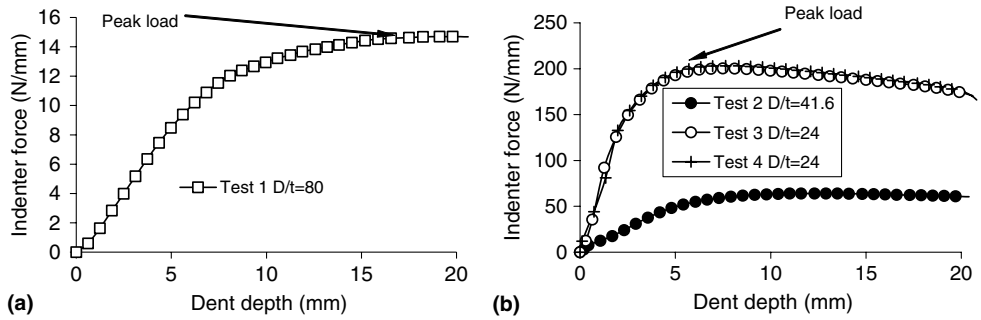

Fig. 4. Indenter force versus dent depth curves for 6082-T6 aluminium alloy rings, obtained from experiments with an offset angle, $\theta_1 = 0°$, a right support angle $\theta_2 = 55°$, and a left support angle $\theta_5 = 35°$.

2.3. Ring test results

The indenter force versus depth curves obtained from the four experiments are shown in Fig. 4. The repeatability of the results is seen to be good from the results obtained for tests TE3 and TE4, which have the same dimensions and test conditions. As the thickness is reduced and hence the D/t value is increased, the peak load drops very significantly and the initial slopes are also reduced.

2.4. FE meshes, boundary conditions

The ABAQUS FE software (ABAQUS, 2003) was used for the analyses. All models consisted of 3600 8-noded plane strain elements with 2×2 integration points, as shown in Fig. 5. This level of mesh refinement was considered adequate for predicting accurate displacements and stresses. However, a coarser mesh may be used if only the displacements are of interest. Alternatively, shell elements can also be used to represent the pipe geometry, see, e.g., Hyde et al. (2001).

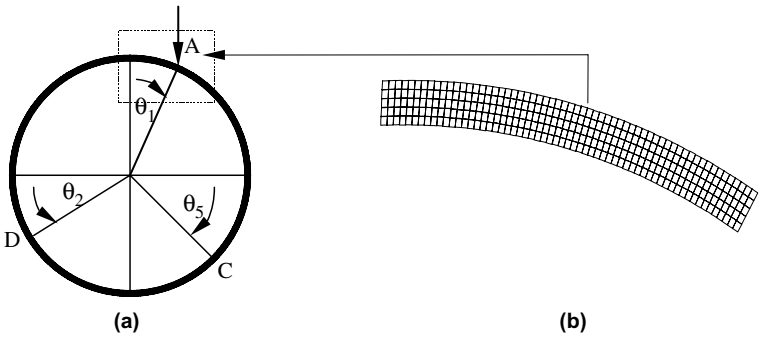

Fig. 5. FE mesh used for the dented ring tests: (a) mesh of a ring and (b) locally amplified mesh.

The rings were fully restrained at the outer diameter at positions C and D. These support points were chosen in order to compare the FE solutions to the analytical solution described in Section 4. The support conditions used in the experiments are only prevented from movement in the outer normal directions of the rings. The indentation load was applied in the vertical downward direction at the outer diameter position at point A.

The loads were applied using a rigid indenter with a 2 mm radius and rigid surface contact elements and assuming that no slipping occurs between the indenter and the rings. The large deformation, elastic–plastic analyses were performed using the standard arc-length (Riks) algorithm facility within ABAQUS.

2.5. Comparison of FE results with the experimental data

The FE predictions are compared with the experimental results in Table 3 and Fig. 6. It can be seen that the FE predictions are slightly higher than the experimental results, but in general, the predictions are in good agreement with the experimental data. The small discrepancy between the FE and experimental results is thought to be due to the fact that the support conditions, on the outer surface of the rings at C and D, used in the FE analyses, were fully fixed whereas the displacements at the same positions in the experiments are only prevented from movements in the outer normal directions of the rings. Hence, the rings used in the

Table 3
D/t ratios, limit loads obtained from the experimental tests and FE

D/t	Limit load (N/mm)		Limit load (N/mm)		Difference (%)
80	TE1	14.9	FE1	15.5	4
41.6	TE2	64.0	FE2	69.5	8.6
24	TE3	203.0	FE3	225	10.8
24	TE4	200.3			12.5

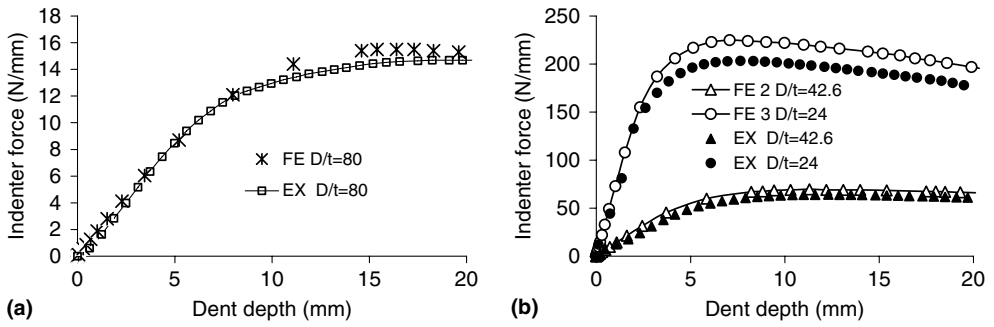

Fig. 6. Comparison of FE predictions with experimental indenter force versus depth curves obtained from the 6082-T6 alloy ring tests with $\theta_1 = 0°$, $\theta_2 = 55°$ and $\theta_5 = 35°$.

FE analyses are subjected to a slightly higher level of constraint than those used for the experiments. However, all of the differences between the FE solutions and the corresponding experimental results are within 13%. This degree of correlation was considered to be good enough and so the same mesh was used for all of the subsequent analyses reported in this paper.

3. Results of general FE analyses

3.1. Materials and geometry

In addition to the FE analyses performed for comparison with the experimental test results for the aluminium alloy (6082-T6), FE analyses were obtained for two other materials. Since practical pipelines are usually made from a variety of steels, FE analyses were performed using material data for one of these steels, namely X65 SAW. An idealised material, Ideal-A, with elastic, perfectly plastic material properties was also used to investigate the influence of material properties on the elastic–plastic response. Ideal-A material has a Young's modulus of 70 GPa and yield stress of 300 MPa. The material properties are summarised in Table 1. In all of the FE analyses, the materials were assumed to obey an isotropic hardening rule. The ring dimensions used in the FE analyses are shown in Table 4. Details of the FE analysis are shown in Tables 5–8.

3.2. Behaviour for pipes made from an idealised elastic perfectly plastic material (Ideal-A)

The idealised elastic perfectly plastic material, Ideal-A, was chosen to investigate the effects of the support and indenter offset angular position on the limit loads. A total of 111 FE analyses (FE4 to FE114) were performed for the Ideal-A material. The typical behaviour obtained from these analyses is as indicated in Fig. 6 which was obtained for the aluminium alloy (FE and experiments). The peak (i.e., limit) loads obtained from analyses (FE4 to FE114) were normalised by dividing them by ($\sigma_y t^2/2R$) and these are shown in Figs. 7–10.

Fig. 7 shows that the peak load slightly increases as the indenter offset angle increases from 0° to 20°. The peak load increases more significantly as the offset angle increases from 20° to 60°. However, at these higher offset angles, it is more likely that slipping will occur between the indenter and the ring. Also, it can be seen, from Figs. 8–10, that the peak load decreases when either the right or left support angle is increased.

3.3. Behaviour of pipes made from X65 SAW steel material

A further 111 FE analyses were performed using the X65 SAW steel material data. The loading and boundary conditions used for the analyses (FE115 to FE225) are given in Tables 6–8. The main reason for perform-

Table 4
Ring dimensions used in the FE analyses

FE model no.	D (mm)	t (mm)	D/t
1	120	1.5	80
2	120	5.0	24
3	128	3.0	42.6
4	88.8	1.2	72
5	92.4	3.0	30.8

Table 5
Ring dimensions, loading and support positions, and limit load solutions obtained from the FE analyses for 6082-T6 aluminium alloy

FE no.	D/t	θ_1 (°)	θ_2 (°)	θ_5 (°)	F_{limit} (N/mm)
FE1	80.0	0	35	55	15.5
FE2	41.6	0	35	55	69.5
FE3	24.0	0	35	55	225

Table 6
Ring dimensions, loading and support positions, and limit load solutions obtained from the FE analyses for the idealised material (ideal-A) and for X65 SAW, for $D/t = 72$

D/t	θ_1 (°)	θ_2 (°)	θ_5 (°)	Idealised-A results		X65 SAW results	
				FE no.	F_{limit} (N/mm)	FE no.	F_{limit} (N/mm)
72.0	0	45	45	FE4	12.7	FE115	24.2
72.0	10	45	45	FE5	12.7	FE116	24.4
72.0	20	45	45	FE6	12.9	FE117	25.0
72.0	30	45	45	FE7	13.9	FE118	26.2
72.0	40	45	45	FE8	15.1	FE119	28.6
72.0	50	45	45	FE9	17.3	FE120	32.7
72.0	60	45	45	FE10	20	FE121	38.2
72.0	20	45	0	FE11	20.8	FE122	39.5
72.0	20	45	10	FE12	18.3	FE123	34.5
72.0	20	45	20	FE13	16.4	FE124	30.9
72.0	20	45	30	FE14	14.8	FE125	28.2
72.0	20	45	40	FE15	13.5	FE126	26.0
72.0	20	45	50	FE16	12.8	FE127	24.1
72.0	20	45	60	FE17	11.7	FE128	22.5
72.0	20	45	70	FE18	11	FE129	21.2
72.0	20	45	80	FE19	10.3	FE130	19.8
72.0	20	45	90	FE20	9.35	FE131	17.9
72.0	20	0	45	FE21	13.8	FE132	26.8
72.0	20	10	45	FE22	13.6	FE133	26.5
72.0	20	20	45	FE23	13.4	FE134	26.1
72.0	20	30	45	FE24	13.2	FE135	25.5
72.0	20	40	45	FE25	13.0	FE136	25.3
72.0	20	50	45	FE26	12.8	FE137	24.8
72.0	20	60	45	FE27	12.6	FE138	24.3
72.0	20	70	45	FE28	12.4	FE139	23.9
72.0	20	80	45	FE29	12.2	FE140	23.4
72.0	20	90	45	FE30	11.7	FE141	22.4
72.0	0	0	45	FE31	15.0	FE142	29.8
72.0	0	10	45	FE32	14.5	FE143	28.3
72.0	0	20	45	FE33	13.9	FE144	27.0
72.0	0	30	45	FE34	13.5	FE145	25.8
72.0	0	40	45	FE35	13	FE146	24.7
72.0	0	50	45	FE36	12.4	FE147	23.7
72.0	0	60	45	FE37	12.0	FE148	22.8
72.0	0	70	45	FE38	11.7	FE149	22.0
72.0	0	80	45	FE39	11.2	FE150	21.2
72.0	0	90	45	FE40	10.4	FE151	19.9

ing these analyses was to investigate the applicability of using a representative nominal flow stress, σ_f, for predicting the peak loads. In this paper, σ_f is taken to be the average of the yield stress and the ultimate tensile stress. As with the idealised material, Ideal-A, the peak loads obtained from X65 SAW steel are normalised by dividing them by $(\sigma_f t^2/2R)$. The results are shown in Figs. 11–14.

A comparison of Figs. 11–14, for the X65 SAW material, with the corresponding results for the Ideal-A material (Figs. 7–10) shows very close correlation. This is more clearly shown in Fig. 15(a)–(d) in which the normalised peak loads for the X65 SAW material are also plotted against the corresponding results obtained for the Ideal-A material, for different indenter offset and support angles. It can be seen, from Fig. 15(a)–(d), that very close correlation of the results is obtained for Ideal-A and X65 SAW steel materials. This indicates that the representative nominal flow stress chosen to normalise the data can be used to predict the peak loads, or limit loads, for hardening materials, from data for idealised elastic–plastic materials (see Hyde et al., 2005a). This conclusion is important when considering the suitability of analytical methods for predicting the behaviour of steel pipes.

Table 7
Ring dimensions, loading and support positions, and limit load solutions obtained from the FE analyses for the idealised material (ideal-A) and for X65 SAW, for $D/t = 42.6$

D/t	θ_1 (°)	θ_2 (°)	θ_5 (°)	Ideal-A results		X65 SAW results	
				FE no.	F_{limit} (N/mm)	FE no.	F_{limit} (N/mm)
42.6	0	45	45	FE41	63	FE152	119
42.6	10	45	45	FE42	63.5	FE153	120.
42.6	20	45	45	FE43	65	FE154	125
42.6	30	45	45	FE44	69	FE155	133.
42.6	40	45	45	FE45	76.5	FE156	145.
42.6	50	45	45	FE46	89	FE157	166
42.6	60	45	45	FE47	107	FE158	199.
42.6	20	45	0	FE48	106	FE159	202
42.6	20	45	10	FE49	92	FE160	176
42.6	20	45	20	FE50	81.5	FE161	157
42.6	20	45	30	FE51	73.5	FE162	142
42.6	20	45	40	FE52	67.5	FE163	130
42.6	20	45	50	FE53	63	FE164	120.
42.6	20	45	60	FE54	59	FE165	112.
42.6	20	45	70	FE55	55.5	FE166	105
42.6	20	45	80	FE56	52	FE167	98
42.6	20	45	90	FE57	46.8	FE168	88
42.6	20	0	45	FE58	71	FE169	134.
42.6	20	10	45	FE59	70	FE170	133
42.6	20	20	45	FE60	68.5	FE171	130.
42.6	20	30	45	FE61	67.5	FE172	128.
42.6	20	40	45	FE62	66	FE173	126
42.6	20	50	45	FE63	64.5	FE174	124
42.6	20	60	45	FE64	63	FE175	121.
42.6	20	70	45	FE65	62	FE176	119.
42.6	20	80	45	FE66	61	FE177	117
42.6	20	90	45	FE67	56.5	FE178	110.
42.6	0	0	45	FE68	75.5	FE179	148.
42.6	0	10	45	FE69	72.5	FE180	140.
42.6	0	20	45	FE70	69.5	FE181	133.
42.6	0	30	45	FE71	67	FE182	127
42.6	0	40	45	FE72	64	FE183	121.
42.6	0	50	45	FE73	62.5	FE184	116.
42.6	0	60	45	FE74	59.5	FE185	112
42.6	0	70	45	FE75	57.5	FE186	108
42.6	0	80	45	FE76	55	FE187	104
42.6	0	90	45	FE77	50.5	FE188	96

4. Analytical methods

4.1. Initial load–displacement gradient

As with the case of symmetrical loading and support conditions for unpressurised pipes (Hyde et al., 2005a), the elastic force–deflection behaviour, for an unpressurised ring, with unsymmetrical loading and support conditions, can be obtained using Castiglano's method. The resulting relationship between force and deflection is given by

$$F = \frac{Et^3}{12R^3}\left(\frac{D}{AD + B + C}\right)\delta \tag{1}$$

where A, B, C and D are functions of the angles θ_2 and θ_5, i.e.,

Table 8
Ring dimensions, loading and support positions and limit load solutions obtained from the FE analyses for the idealised material (ideal-A) and for X65 SAW, for $D/t = 30.8$

D/t	θ_1 (°)	θ_2 (°)	θ_5 (°)	Ideal-A results		X65 SAW results	
				FE no.	F_{limit} (N/mm)	FE no.	F_{limit} (N/mm)
30.8	0	45	45	FE78	90.5	FE189	170.
30.8	10	45	45	FE79	91	FE190	177.
30.8	20	45	45	FE80	92.5	FE191	179
30.8	30	45	45	FE81	99	FE192	190.
30.8	40	45	45	FE82	111	FE193	203.
30.8	50	45	45	FE83	128.	FE194	237.
30.8	60	45	45	FE84	152.	FE195	284
30.8	20	45	0	FE85	153.	FE196	292
30.8	20	45	10	FE86	133.	FE197	254.
30.8	20	45	20	FE87	117	FE198	226
30.8	20	45	30	FE88	104.	FE199	203.
30.8	20	45	40	FE89	96	FE200	186
30.8	20	45	50	FE90	89.5	FE201	172
30.8	20	45	60	FE91	83.5	FE202	160
30.8	20	45	70	FE92	78	FE203	149
30.8	20	45	80	FE93	73	FE204	138.
30.8	20	45	90	FE94	66.5	FE205	124.
30.8	20	0	45	FE95	101	FE206	192
30.8	20	10	45	FE96	99	FE207	189.
30.8	20	20	45	FE97	97.5	FE208	186.
30.8	20	30	45	FE98	95	FE209	183.
30.8	20	40	45	FE99	93.5	FE210	180.
30.8	20	50	45	FE100	91.5	FE211	177.
30.8	20	60	45	FE101	90	FE212	174.
30.8	20	70	45	FE102	88.5	FE213	171.
30.8	20	80	45	FE103	86.5	FE214	167.
30.8	20	90	45	FE104	81.5	FE215	157.
30.8	0	0	45	FE105	109.	FE216	214
30.8	0	10	45	FE106	104.	FE217	202
30.8	0	20	45	FE107	100	FE218	191
30.8	0	30	45	FE108	96	FE219	182
30.8	0	40	45	FE109	92	FE220	174
30.8	0	50	45	FE110	88.5	FE221	167
30.8	0	60	45	FE111	85.5	FE222	160.
30.8	0	70	45	FE112	82	FE223	154.
30.8	0	80	45	FE113	78.5	FE224	148
30.8	0	90	45	FE114	72	FE225	136.

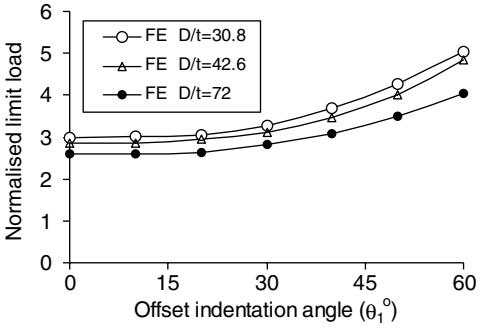

Fig. 7. The normalised peak load versus indenter offset angular position, with $\theta_2 = \theta_5 = 45°$ and $D/t = 72$, 42.6 and 30.8, for idealised material Ideal-A.

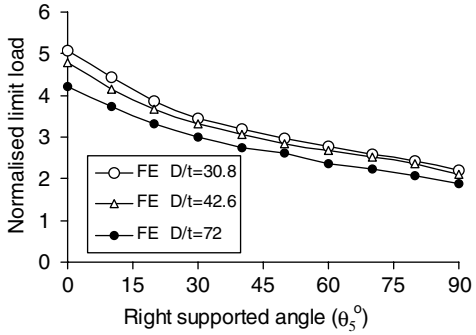

Fig. 8. The normalised peak load versus right support angular position, with $\theta_2 = 45°$, $D/t = 72$, 42.6 and 30.8 and $\theta_1 = 20°$, for idealised material Ideal-A.

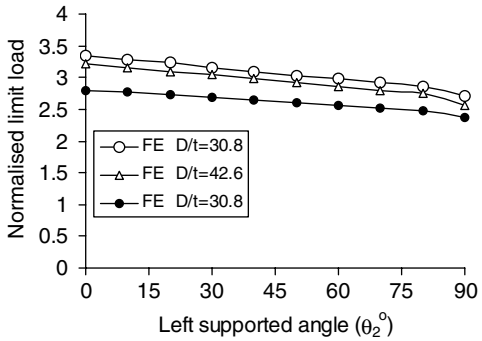

Fig. 9. The normalised peak load versus left support angular position, with $\theta_5 = 45°$, $D/t = 72$, 42.6 and 30.8 and $\theta_1 = 20°$, for idealised material Ideal-A.

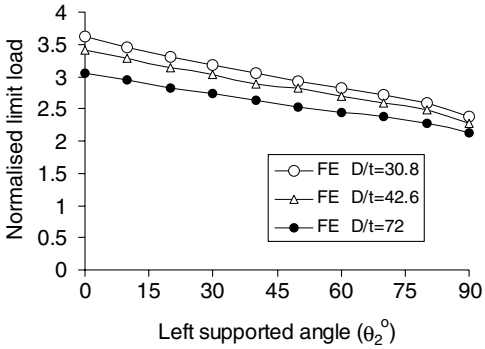

Fig. 10. The normalised peak load versus left support angular position, with $\theta_5 = 45°$, $D/t = 72$, 42.6 and 30.8 and $\theta_1 = 0°$, for idealised material Ideal-A.

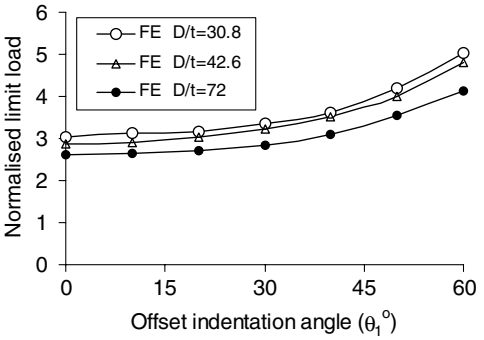

Fig. 11. The normalised peak load versus indenter offset angular position, with $\theta_2 = \theta_5 = 45°$ and $D/t = 72$, 42.6 and 30.8, for X65 SAW steel.

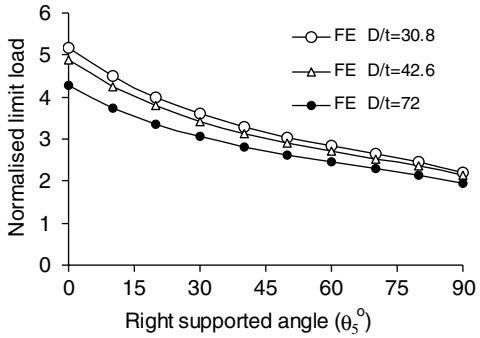

Fig. 12. The normalised peak load versus right support angular position, with $\theta_2 = 45°$, $D/t = 72$, 42.6 and 30.8 and $\theta_1 = 20°$, for X65 SAW steel.

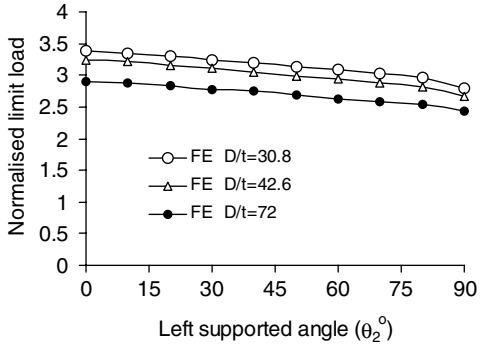

Fig. 13. The normalised peak load versus left supported angular position, with $\theta_5 = 45°$, $D/t = 72$, 42.6 and 30.8 and $\theta_1 = 20°$, for X65 SAW steel.

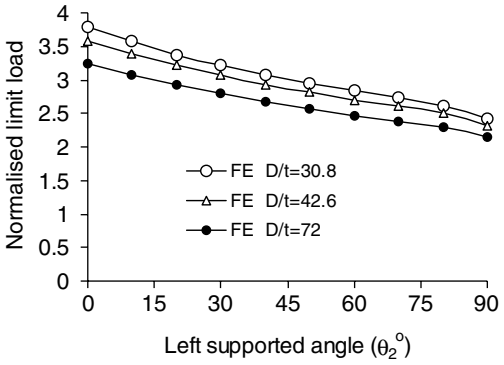

Fig. 14. The normalised peak load versus left support angular position, with $\theta_5 = 45°$, $D/t = 72$, 42.6 and 30.8 and $\theta_1 = 0°$, for X65 SAW steel.

$$
\begin{aligned}
A &= \frac{1}{8}\left(\pi + \theta_2 + \theta_5 + \frac{1}{2}(\sin 2\theta_2 + \sin 2\theta_5)\right)\\
B &= \left(1 + \frac{1}{2}\sin\theta_2 + \frac{1}{2}\sin\theta_5\right)(B1 + B2 + B3)\\
B1 &= \sin 2\theta_2 + \sin 2\theta_5 + \sin(\theta_2 + \theta_5) + \left(3 + \frac{1}{2}\sin\theta_2 \sin\theta_5\right)(\cos\theta_2 + \cos\theta_5)\\
B2 &= -\frac{1}{2}(\pi + \theta_2 + \theta_5)(\cos^2\theta_2 + \sin\theta_2 + \cos^2\theta_5 + \sin\theta_5 + 2)\\
B3 &= -\frac{1}{2}\cos\theta_2 \sin^2\theta_5 - \frac{1}{2}\sin^2\theta_2 \cos\theta_5\\
C &= \frac{1}{4}\left(1 + \frac{1}{2}\sin^2\theta_2 + \sin\theta_2 + \frac{1}{2}\sin^2\theta_5 + \sin\theta_5\right)(C1 + C2)\\
C1 &= (\pi + \theta_2 + \theta_5)(\cos^2\theta_2 + \cos^2\theta_5)\\
C2 &= -\sin 2\theta_2 - \sin 2\theta_5 - 2\sin(\theta_2 + \theta_5) - 4\cos\theta_2 - 4\cos\theta_5\\
D &= \frac{1}{2}(\pi + \theta_2 + \theta_5)^2 - (\cos\theta_2 + \cos\theta_5)^2 - \frac{1}{4}(\pi + \theta_2 + \theta_5)(\sin 2\theta_2 + \sin 2\theta_5)
\end{aligned}
\tag{2}
$$

Hence, the initial slope, K, of the indenter force versus depth curves, for an unpressurised ring with unsymmetrical loading and support condition, is given by

$$K = \frac{Et^3}{12R^3}\left(\frac{D}{AD + B + C}\right) \tag{3}$$

Fig. 16 shows a typical comparison between the initial gradients obtained from the FE and experimental tests with the analytical predictions. It can be seen that the agreement is excellent. This degree of accuracy is applicable to all of the materials, geometries, load positions and support positions investigated.

4.2. Upper bound limit load theory

As in the case of symmetrical support and radial loading conditions, discussed in Hyde et al. (2005a), FE analysis indicated that the offset indentation resulted in the ring having five distinct plastic regions. Hence, in order to determine the upper bound, it was assumed that the offset indenter ring has five plastic hinges, at positions A, B, C, D and E, as shown in Fig. 17(a). The rotational angles of these five plastic hinges (A, B, C, D and E) are denoted as α_5, α_2, α_1, α_3 and α_4, respectively, as shown in Fig. 17(b). If the load point, position A, moves vertically downwards, as shown in Fig. 17(b), the relationships between the angles of rotation and the load line

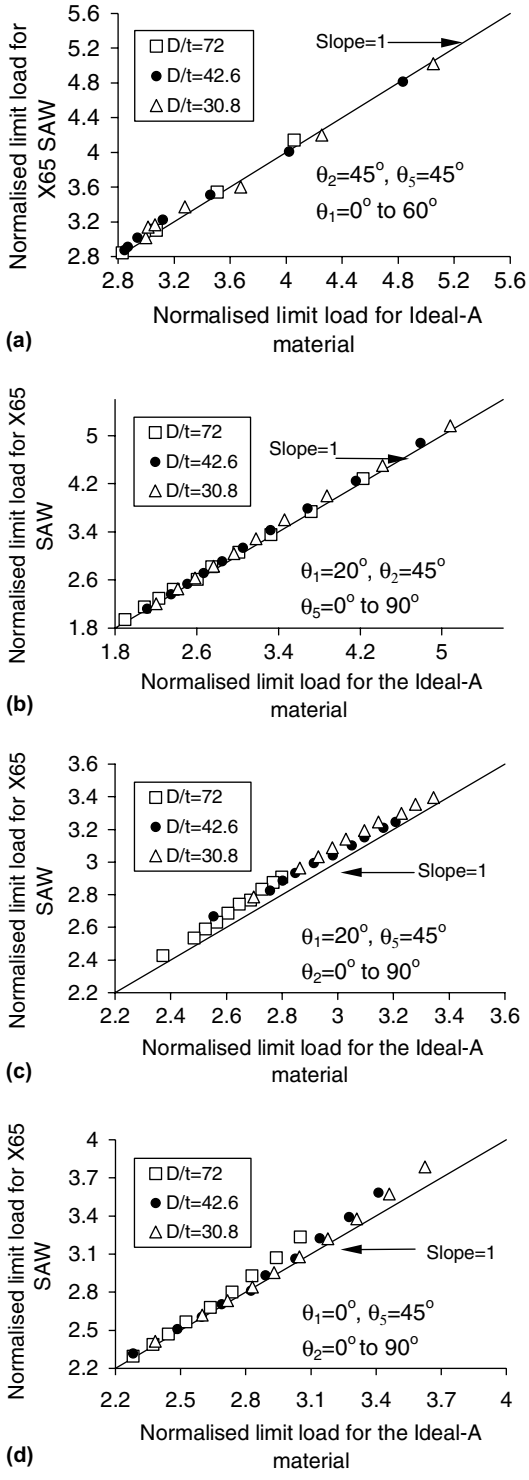

Fig. 15. FE normalised peak loads for X65 SAW steel versus those for 6082-T6 aluminium alloy, for different indenter offset angular positions, different support angular positions and for different D/t ratios.

displacement can be determined and hence the upper bound analysis method, previously used for symmetrical support and loading (Hyde et al., 2005a,b), can again be used.

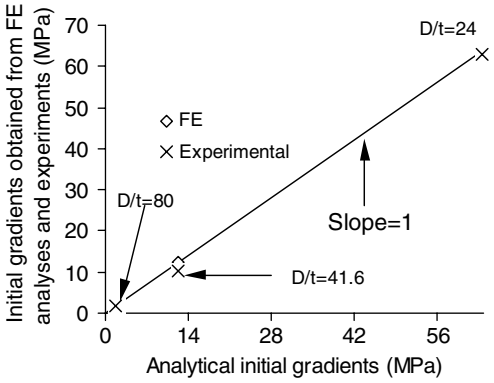

Fig. 16. A comparison of initial gradients of the indenter force versus dent depth curves obtained from the FE analyses, the experimental test data and the analytical methods for 6082-T6 aluminium alloy ring models with $D/t = 80$, 41.6 and 24, $\theta_1 = 0°$, $\theta_2 = 55°$ and $\theta_5 = 35°$.

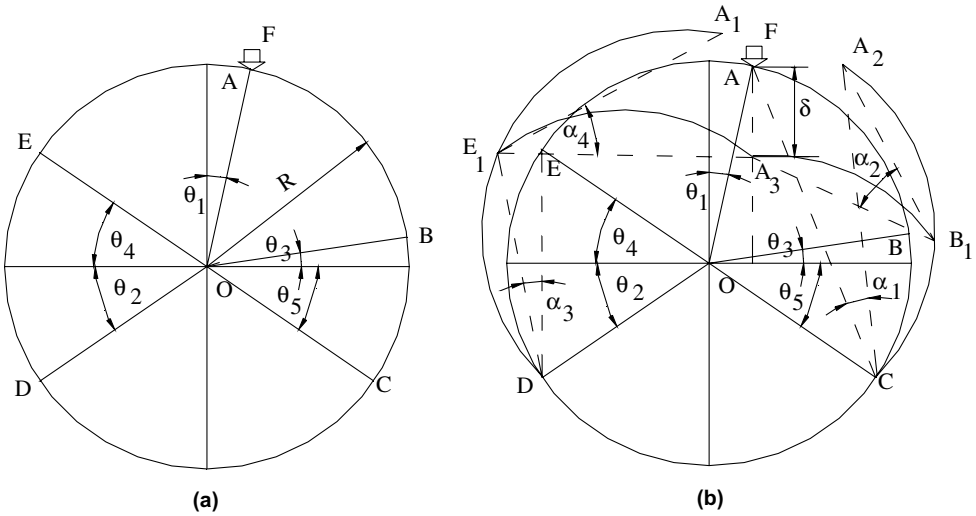

Fig. 17. Kinematically admissible velocity field for the upper bound analysis. (a) Offset indented ring and (b) deformation of offset indented ring.

To determine the upper bound, the angles of the plastic hinge rotation and the line displacement are assumed to be very small. On the basis of the geometric compatibility of the deformations, the kinematic relationships can be represented by the following equations:

$$\mathrm{d}\alpha_2 = \frac{\cos\theta_1 + \sin\theta_5}{\cos\theta_1 - \sin\theta_3}\,\mathrm{d}\alpha_1 \tag{4a}$$

$$\mathrm{d}\alpha_4 = \frac{\cos\theta_1 + \sin\theta_2}{\cos\theta_1 - \sin\theta_4}\,\mathrm{d}\alpha_3 \tag{4b}$$

$$\mathrm{d}\alpha_5 = \mathrm{d}\alpha_2 + \mathrm{d}\alpha_4 - \mathrm{d}\alpha_1 - \mathrm{d}\alpha_3 \tag{4c}$$

$$\mathrm{d}\delta = R\frac{\cos(\theta_4 - \theta_1) - \cos(\theta_2 - \theta_1) + \sin(\theta_2 + \theta_4)}{\cos\theta_1 - \sin\theta_4}\,\mathrm{d}\alpha_3 \tag{4d}$$

$$\mathrm{d}\delta = R\frac{\cos(\theta_3 + \theta_1) - \cos(\theta_5 + \theta_1) + \sin(\theta_5 + \theta_3)}{\cos\theta_1 - \sin\theta_3}\,\mathrm{d}\alpha_1 \tag{4e}$$

From Eqs. (4d) and (4e), it follows that

$$d\alpha_3 = \frac{\cos\theta_1 - \sin\theta_4}{\cos\theta_1 - \sin\theta_3}\frac{\cos(\theta_3+\theta_1) - \cos(\theta_5+\theta_1) + \sin(\theta_5+\theta_3)}{\cos(\theta_4-\theta_1) - \cos(\theta_2-\theta_1) + \sin(\theta_2+\theta_4)}\,d\alpha_1 \tag{5}$$

Substituting Eq. (5) into (4b) gives

$$d\alpha_4 = \frac{\cos\theta_1 + \sin\theta_2}{\cos\theta_1 - \sin\theta_3}\frac{\cos(\theta_3+\theta_1) - \cos(\theta_5+\theta_1) + \sin(\theta_5+\theta_3)}{\cos(\theta_4-\theta_1) - \cos(\theta_2-\theta_1) + \sin(\theta_2+\theta_4)}\,d\alpha_1 \tag{6}$$

The internal energy dissipated, W_I, at the plastic hinges, is given by

$$W_I = M_0(d\alpha_1 + d\alpha_2 + d\alpha_3 + d\alpha_4 + d\alpha_5) \tag{7}$$

where

$$M_0 = \frac{1}{4}\sigma_y t^2 \tag{8}$$

where t is the ring wall thickness and σ_y is the material yield stress.

Substituting for $d\alpha_2$, $d\alpha_3$, $d\alpha_4$ and $d\alpha_5$ from Eqs. (4a), (5), (4b) and (4c) into (7) gives

$$W_I = 2M_0\left[\frac{\cos\theta_1 + \sin\theta_5}{\cos\theta_1 - \sin\theta_3} + \frac{\cos\theta_1 + \sin\theta_2}{\cos\theta_1 - \sin\theta_3}\frac{\cos(\theta_3+\theta_1) - \cos(\theta_5+\theta_1) + \sin(\theta_5+\theta_3)}{\cos(\theta_4-\theta_1) - \cos(\theta_2-\theta_1) + \sin(\theta_2+\theta_4)}\right]d\alpha_1 \tag{9}$$

Based on Eqs. (4d) and (4e), the work done, W_E, by the external force, F, is given by

$$W_E = F\,d\delta = RF\frac{\cos(\theta_3+\theta_1) - \cos(\theta_5+\theta_1) + \sin(\theta_5+\theta_3)}{\cos\theta_1 - \sin\theta_3}\,d\alpha_1 \tag{10}$$

Since the work done by the external force is equal to the internal energy dissipated, then Eqs. (9) and (10) give

$$F = 2M_0 \times \frac{1}{R}\left[\frac{\cos\theta_1 + \sin\theta_5}{\cos(\theta_3+\theta_1) - \cos(\theta_5+\theta_1) + \sin(\theta_5+\theta_3)} + \frac{\cos\theta_1 + \sin\theta_2}{\cos(\theta_4-\theta_1) - \cos(\theta_2-\theta_1) + \sin(\theta_2+\theta_4)}\right] \tag{11}$$

Minimising the external force F with respect to θ_3 and θ_4, the optimised upper bound, F_U, is given by

$$F_U = 2M_0\frac{1}{R}L_s(\theta_1,\theta_2,\theta_5) \tag{12}$$

where $L_s(\theta_1,\theta_2,\theta_5)$ is a normalised function of θ_1, θ_2 and θ_3, given by

$$L_s(\theta_1,\theta_2,\theta_5) = \frac{\cos\theta_1 + \sin\theta_2}{2\sin\left(\frac{\pi}{4} + \frac{\theta_2+\theta_1}{2}\right) - \cos(\theta_2+\theta_1)} + \frac{\cos\theta_1 + \sin\theta_5}{2\sin\left(\frac{\pi}{4} + \frac{\theta_5-\theta_1}{2}\right) - \cos(\theta_5-\theta_1)} \tag{13}$$

If taking $\theta_2 = \theta_5$ and $\theta_3 = \theta_4$, then $\theta_1 = 0$ and Eq. (13) becomes:

$$L_s(\theta_2) = \frac{2(1+\sin\theta_2)}{2\sin\left(\frac{\pi}{4} + \frac{\theta_2}{2}\right) - \cos\theta_2} \tag{14}$$

which is the same as the solution for an unpressurised pipe with symmetrical supports, as shown in Hyde et al. (2005a). It can be seen that the solution presented in Hyde et al. (2005a) is a special case of the offset indentation studied in this paper.

5. Comparison of the analytical solutions with the FE and experimental results

5.1. 6082-T6 alloy results

The indenter force versus dent depth curves, obtained from the FE analyses and experimental tests performed on the aluminium alloy models, are shown in Fig. 18. The analytical limit load solutions, also shown in Fig. 18, were calculated by using a representative nominal flow stress which is the average of the yield stress

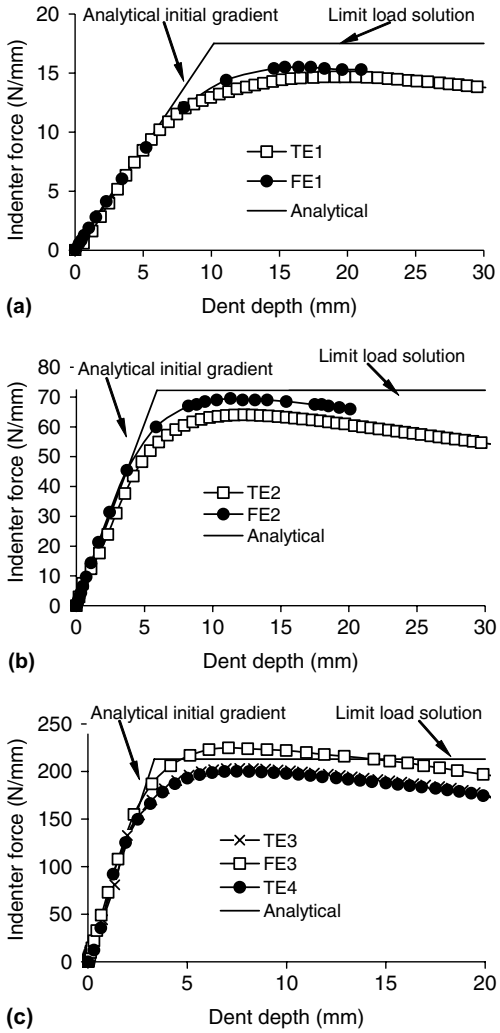

Fig. 18. Indenter force versus dent depth curves obtained from the FE analyses, experimental tests and the analytical methods, for the case with $\theta_1 = 0°$, $\theta_2 = 55°$ and $\theta_5 = 35°$, for the 6082-T6 aluminium alloy rings (a) $D/t = 80$ (b) $D/t = 41.6$ (c) $D/t = 30.8$.

and the ultimate tensile stress. The analytical, elastic solutions for the initial load–displacement gradient, also shown in Fig. 18, are obtained using Eq. (1). The limit loads, obtained from the FE and analytical analyses, are also given in Table 9, which shows that the analytical limit loads, obtained using the nominal flow stress in the predictions, are generally in reasonably good agreement with those obtained from the experiments and the FE analyses. However, these data indicate that if a slightly lower representative flow stress was used for the analytical predictions, then generally closer correlation between the analytical solutions and those obtained from the FE analyses and experimental tests would be obtained.

Table 9
FE, experimental and analytical limit loads for 6082-T6 aluminium alloy rings using yield, flow and ultimate tensile stresses in the analytical formulations (σ_y = yield stress; σ_f = flow stress; σ_{UTS} = ultimate tensile stress) for $\theta_1 = 0°$, $\theta_2 = 55°$ and $\theta_5 = 35°$

D/t	Experimental (N/mm)		FE (N/mm)	Analytical using σ_y	Analytical using σ_f	Analytical using σ_{UTS}
80	TE1	14.69	15.5	17	18.4	19.8
41.6	TE2	64.03	69.5	66.6	72.3	77.9
24	TE3	203.25	225	196.3	213.	229.7
	TE4	200.29				

5.2. Ideal-A results

The peak loads obtained from each of the FE analyses, using the elastic perfectly plastic material model (Ideal-A) and from the theoretical analyses, are normalised by dividing them by ($\sigma_y t^2/2R$); the results are shown in Figs. 19–22.

Figs. 19–22 show that for the smaller D/t ratios, i.e., $D/t = 41.6$ and 30.8, very close correlation of the FE and the analytical solutions can be obtained. However, for the larger D/t ratios, i.e., $D/t = 80$, the FE solutions are significantly lower than the corresponding analytical solutions. This is because large non-linear deformation effects which occur in the large D/t ratio rings, is included in the FE analyses but not in the analytical solutions. Therefore, for the peak load predictions of large D/t ratios, it is suggested that the yield stress should be used in the analytical method (see Hyde et al., 2005a).

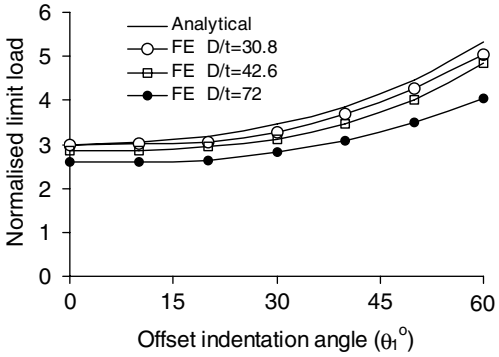

Fig. 19. A comparison of the FE and analytical normalised limit loads for different offset angular positions, with $\theta_2 = \theta_5 = 45°$, for the idealised material Ideal-A.

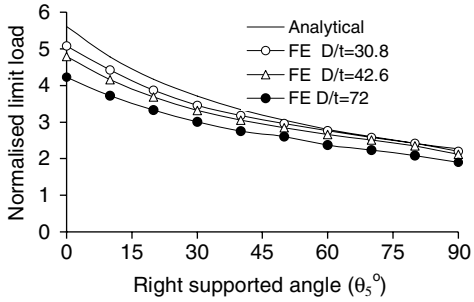

Fig. 20. A comparison of the FE and analytical normalised limit loads for different right support angular positions, with $\theta_1 = 20°$ and $\theta_2 = 45°$, for the idealised material Ideal-A.

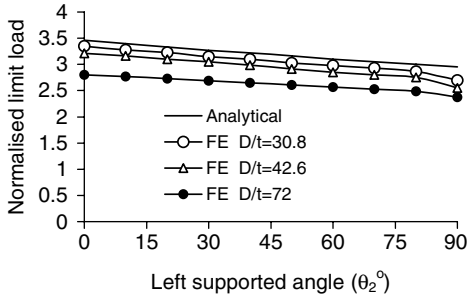

Fig. 21. A comparison of the FE and analytical normalised limit loads for different left support angular positions, with $\theta_1 = 20°$ and $\theta_5 = 45°$, for the idealised material Ideal-A.

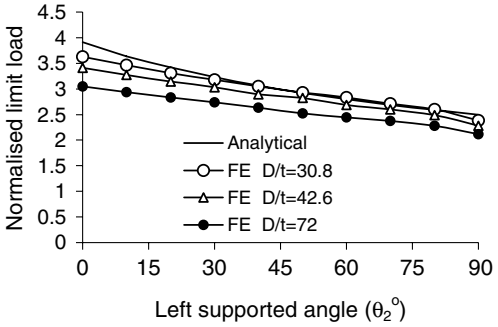

Fig. 22. A comparison of the FE and analytical normalised limit loads for different left support angular positions, with $\theta_1 = 0°$ and $\theta_5 = 45°$, for the idealised material Ideal-A.

5.3. X65 SAW steel results

The normalised limit loads obtained from each of the FE analyses for the X65 SAW steel models are compared with those obtained for the idealised material Ideal-A in Fig. 15(a)–(d). The close correlation of the results indicates that the normalised limit loads can be obtained either using the idealised material Ideal-A or using the X65 SAW steel models in the FE analyses. The normalised limit loads obtained from the FE analyses and the analytical methods for the idealised material Ideal-A are the same as those for the X65 SAW steel. Comparisons of the peak loads, obtained from the FE analyses, and the analytical solutions are shown in Figs. 23–26 for the X65 SAW steel material. It can be seen from Figs. 23–26 that a reasonably close correlation

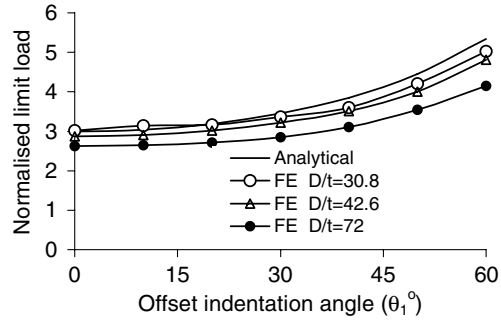

Fig. 23. A comparison of the FE and analytical normalised limit loads for different offset angular positions, with $\theta_2 = \theta_5 = 45°$, for X65 SAW steel material.

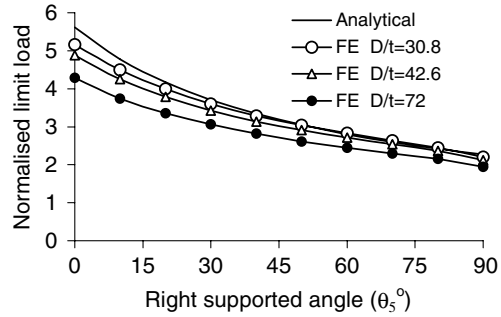

Fig. 24. A comparison of the FE and analytical normalised limit loads for different right support angular positions, with $\theta_1 = 20°$ and $\theta_2 = 45°$, for X65 SAW steel material.

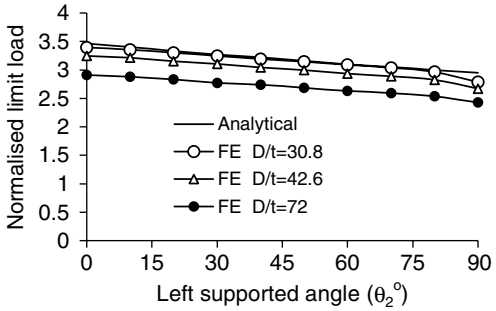

Fig. 25. A comparison of the FE and analytical normalised limit loads for different left support angular positions, with $\theta_1 = 20°$ and $\theta_5 = 45°$, for X65 SAW steel material.

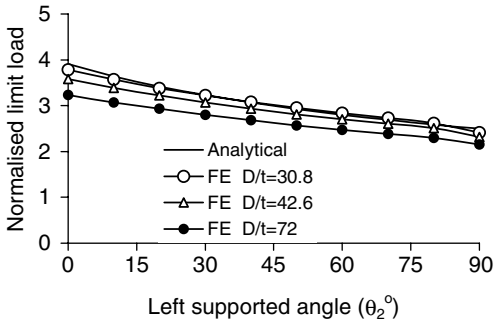

Fig. 26. A comparison of the FE and analytical normalised limit loads for different left support angular positions, with $\theta_1 = 0°$ and $\theta_5 = 45°$, for X65 SAW steel material.

exists between the analytical solutions and the FE predictions of the peak loads for the X65 SAW steel material.

6. Conclusions

The reasonably close correlation between the FE predictions of indenter force versus depth and the corresponding experimental test data indicates that large deformation non-linear FE analysis is capable of producing accurate results.

An upper bound limit load analytical approach for predicting the peak (or limit) loads gives good (i.e., close to the FE results) upper bounds for rings with elastic perfectly plastic material behaviour models. The correlation is generally good but is poorest for the larger D/t ratios because the analytical approach does not model the significant effect of the large deformations which occur with large D/t ratios.

Using a representative nominal flow stress, which is the average of the yield stress and ultimate tensile stress, a reasonably good correlation between the analytical and FE predictions, for rings made from 6082-T6 aluminium alloy and X65 SAW steel, are obtained. For higher D/t ratios, better correlation would be obtained if the yield stress is used to predict the limit loads using the analytical approach.

The initial slope and peak values of the force versus dent depth curves can be accurately predicted using simple analytical approaches. Use of the simple analytical approaches could significantly reduce the time and effort required in assessing the likely effects on the structural integrity of dents created in pipelines due to accidents.

However, since impact damage of a short 3D indenter is very localised, a pipe with a short indenter may burst or rupture before collapsing, due to a high stress concentration on the edge of the indentation. Hence it is expected that the force–deflection behaviour of a 2D ring with a long indenter will be different from an indented pipe with a short 3D indenter.

Acknowledgements

The authors wish to acknowledge the financial support and technical direction of Advantica and the University of Nottingham, for this work, through the University of Nottingham/Advantica joint scholarship awarded to Dr. Luo. The opinions expressed in this paper do not necessarily represent those of Advantica.

References

ABAQUS version 6.3, ABAQUS Inc., 2003.

Alexander, C.R., 1999. Analysis of dented pipes considering constrained and unconstrained dent configurations. In: Energy Sources and Technology Conference, ASME, ETCE99-6686.

Clapham, L., Mandal, K., Sabet-Sharghi, R., Atherton, D.L., Holden, T., 1998. Variations in stress concentration factors near simulated corrosion pits as monitored by magnetic flux leakage, magnetic Barkhausen noise and neutron diffraction. International Pipeline Conference, vol. 1. ASME, pp. 505–512.

Corder, I., Chatain, P., 1995. EPRG recommendations for the assessment of the resistance of pipelines to external damage. AGA/EPRG Seminar, England.

Doglione, R., Firrao, D., 1998. Structure collapse calculations of old pipelines. Int. J. Fatigue 20, 161–168.

Fowler, J.R., Alexander, C.R., Kovach, P.J., Connelly, L.M., 1995. Fatigue life of pipelines with dents and gouges subjected to cyclic internal pressure. American Society of Mechanical Engineers, Petroleum Division, PD vol. 69, pp. 17–35.

Hyde, T.H., Luo, R., Becker, A.A., 2001. Finite element analysis of indented pipes using three-dimensional solid and shell elements. In: Proc. International Gas Research Conference, Amsterdam, 5–8 November. Gas Technology Institute, Illionois, Omnipress.

Hyde, T.H., Luo, R., Becker, A.A., 2005a. Elastic–plastic response of unpressurised pipes subjected to axially-long radial indentation. Int. J. Mech. Sci. 47, 1949–1971.

Hyde, T.H., Luo, R., Becker, A.A., 2005b. Prediction of force–deflection behaviour of pressurised pipes subjected to axially long radial indentation. Int. J. Pressure Vessels Piping 82, 625–637.

Hyde, T.H., Luo, R., Becker, A.A., 2006. Force–deflection analysis of offset indentations on pressurised pipes. Int. J. Pressure Vessels Piping, in press.

Kiefner, J.F., Alexander, C.R., Fowler, J.R., 1996. Repair of dents containing minor scratches, 9th symposium on pipeline research, PRC International, American Gas Association, paper 5, pp. 1–21.

Lancaster, E.R., Palmer, S.C., 1996a. Burst pressures of pipes containing dents and gouges. Proc. Inst. Mech. Eng., Part E: J. Proc. Mech. Eng. 210 (E1), 19–27.

Lancaster, E.R., Palmer, S.C., 1996b. Strain concentrations in pressured dented pipes. Proc. Inst. Mech. Eng., Part E: J. Proc. Mech. Eng. 210 (E1), 29–38.

Leis, B.N., Francini, R.B., Mohan, R., Rudland, D.L., Olson, R.J., 1998. Pressure–displacement behaviour of transmission pipelines under outside forces-towards a serviceability criterion for mechanical damage. Proc. Int. Offshore Polar Eng. Conf. 2, 60–67.

Park, T.D., Kyriakides, S., 1996. On the collapse of dented cylinders under external pressure. Int. J. Mech. Sci. 38, 557–578.